

Spitzer Observations of the Type Ia Supernova Remnant N103B: Kepler's Older Cousin?

Brian J. Williams,^{1,2} Kazimierz J. Borkowski,³ Stephen P. Reynolds,³ Parviz Ghavamian,⁴ John C. Raymond,⁵ Knox S. Long,⁶ William P. Blair,⁷ Ravi Sankrit,⁸ P. Frank Winkler⁹ & Sean P. Hendrick¹⁰

Received _____; accepted _____

¹NASA Goddard Space Flight Center, Greenbelt, MD 20771; brian.j.williams@nasa.gov

²NASA Postdoctoral Program Fellow

³Physics Dept., North Carolina State University, Raleigh, NC 27695-8202.

⁴Dept. of Physics, Chemistry, and Geosciences, Towson University, Towson, MD 21252

⁵Harvard-Smithsonian Center for Astrophysics, 60 Garden Street, Cambridge, MA 02138.

⁶STScI, 3700 San Martin Dr., Baltimore, MD 21218

⁷Dept. of Physics and Astronomy, Johns Hopkins University, 3400 N. Charles St., Baltimore, MD 21218-2686

⁸SOFIA/USRA

⁹Dept. of Physics, Middlebury College, Middlebury, VT 05753

¹⁰Physics Dept., Millersville U., PO Box 1002, Millersville, PA 17551

ABSTRACT

We report results from *Spitzer* observations of SNR 0509-68.7, also known as N103B, a young Type Ia supernova remnant in the Large Magellanic Cloud that shows interaction with a dense medium in its western hemisphere. Our images show that N103B has strong IR emission from warm dust in the post-shock environment. The post-shock gas density we derive, 45 cm^{-3} , is much higher than in other Type Ia remnants in the LMC, though a lack of spatial resolution may bias measurements towards regions of higher than average density. This density is similar to that in Kepler’s SNR, a Type Ia interacting with a circumstellar medium. Optical images show $\text{H}\alpha$ emission along the entire periphery of the western portion of the shock, with [O III] and [S II] lines emitted from a few dense clumps of material where the shock has become radiative. The dust is silicate in nature, though standard silicate dust models fail to reproduce the “18 μm ” silicate feature that peaks instead at 17.3 μm . We propose that the dense material is circumstellar material lost from the progenitor system, as with Kepler. If the CSM interpretation is correct, this remnant would become the second member, along with Kepler, of a class of Type Ia remnants characterized by interaction with a dense CSM hundreds of years post-explosion. A lack of N enhancement eliminates symbiotic AGB progenitors. The white dwarf companion must have been relatively unevolved at the time of the explosion.

1. Introduction

While the importance of Type Ia supernovae (SNe) in astrophysics is widely known, there are significant uncertainties in the nature of the progenitor systems and the explosions themselves. There is now significant debate in the literature over whether these SNe result

from single-degenerate (the explosion of a white dwarf that has accreted matter close to the Chandrasekhar mass of $1.4 M_{\odot}$ from a companion) or double-degenerate (the merger of two sub-Chandrasekhar mass white dwarfs) systems. In the last few years, most studies have favored a double-degenerate origin for most SNe Ia; Gilfanov & Bogdan (2010) claim that 95% of SNe Ia must result from this progenitor system. Wang & Han (2012) provide a thorough review of the possible explosion mechanisms for Type Ia SNe.

Recently, particular attention has been paid to a growing subclass of extragalactic Type Ia SNe that show signs of interaction with material in a circumstellar medium (CSM) at early times (Silverman et al. 2013). Although only about a dozen of these objects have been observed, the host galaxies are all late-type spirals like the Milky Way or dwarf irregulars like the Large Magellanic Cloud (LMC), implying an origin in relatively young stellar populations (Silverman et al. 2013). Observations of these SNe imply that the surrounding CSM is quite dense; however, to date, no radio or X-ray emission has been observed (likely due to their being too far away). Supernova remnants (SNRs), on the other hand, may be able to manifest the presence of CSM hundreds or even thousands of years after the explosion.

We report here on Spitzer imaging and spectroscopic observations of N103B, a small ($\sim 15''$ radius, or ~ 3.6 pc at a distance of 50 kpc) SNR in the LMC. Light echoes from the remnant place its age at ~ 870 years (Rest et al. 2005), or about twice as old as Kepler’s SNR. As we show in this paper, this remnant bears some strong resemblances to Kepler’s SNR in our Galaxy, so much so that we propose that it may be a Kepler analog at 50 kpc.

Also known as SNR 0509-68.7, N103B is not without its share of controversy. Arguments for a Type Ia origin have been made by several authors. Hughes et al. (1995) examined *ASCA* spectra and found a high Fe/O ratio in the X-ray spectra. Lewis et al. (2003) verified this result with *Chandra* observations. Lopez et al. (2011) conducted a statistical analysis of the morphology of the remnant and concluded that the overall shape of the emission was more consistent with

that of Type Ia SNRs in both the LMC and the Galaxy. Yang et al. (2013) favor a Type Ia origin based on the strength of Cr and Mn lines in the spectrum and their relative strength compared to Fe. Additionally, Badenes et al. (2009) favor a Type Ia SNR, noting that the remnant is associated with a region of the LMC that underwent recent star formation, implying that the progenitor, like Kepler, might have had a relatively young, massive progenitor with substantial mass loss prior to explosion. They suggest that the structure of the remnant may be due to CSM interaction. Finally, no compact remnant or pulsar wind nebula has ever been observed in the remnant, whereas many known core-collapse (CC) SNRs in the LMC do have known neutron stars or pulsars (a notable exception to this is SN 1987A, where no compact remnant has yet been observed).

On the other hand, Van der Heyden et al. (2002) argue in favor of a CC supernova origin for N103B based on the presence of O lines in the *XMM-Newton* RGS spectra. Most recently, Someya et al. (2013) find that the *Suzaku* X-ray spectra are best fit with H-dominated plasmas that more likely originate in Type II SNe. They find that the abundances in this model are most consistent with a $13 M_{\odot}$ progenitor.

However, recently obtained light echo spectroscopy has settled the issue. Rest et al. (in preparation) show that the spectra of the light echos from N103B, first reported in Rest et al. (2005), are consistent with a SN Ia. *Light echo confirmation of the SN type is something that not even Kepler has.*

From the SNR perspective, remnants of Type Ia SNe can generally be modeled without invoking a dense or complex CSM in their surroundings (Badenes et al. 2007). Most Type Ia remnants, such as SN 1006, are evolving into a rather low-density ISM (Katsuda et al. 2013; Winkler et al. 2013). Other examples of such remnants include Tycho’s SNR (Williams et al. 2013), SNR 0509-67.5 (Williams et al. 2011), and SN 1885 in M31 (Badenes et al. 2007). Searches for potential companion stars to these SNe have come up empty (e.g., Schaefer & Pagnotta 2012; Kerzendorf et al. 2014). The simplest explanation for these (and

indeed, most) Type Ia remnants is the double-degenerate scenario described above.

There are a few outliers: RCW 86 appears to have exploded into a low density, wind-blown cavity (Williams et al. 2011b), implying an single-degenerate scenario. Kepler’s SNR, on the other hand, has extremely dense surroundings, indicative of CSM material. Blair et al. (2007) and Williams et al. (2012) used *Spitzer* imaging and spectroscopic observations to quantify the high densities in Kepler. From the spectral signatures of the dust observed, they concluded that an O-rich AGB star must have been part of the progenitor system. Reynolds et al. (2007) and Burkey et al. (2013) concluded from *Chandra* X-ray observations that Kepler was an example of a “prompt” Type Ia SN; i.e., a progenitor that exploded within a few hundred Myr of forming, and that the remnant is most consistent with a progenitor system which blew a dense, equatorial wind prior to exploding, a situation which implies a single-degenerate progenitor scenario. Thus far, Kepler’s SNR is the only remnant known with a dense CSM; finding others will bridge the gap between SNe Ia-CSM and their remnants.

We organize this paper in the following fashion. In Section 2, we detail the infrared and optical observations and data reduction. In Section 3, we report the results of our analysis. Section 4 provides a discussion of our interpretation of our results. Section 5 serves as a summary of our findings.

2. Observations

Spitzer imaging observations of N103B were carried out as part of Program ID 3680. We observed the remnant in all bands of both the Infrared Array Camera (IRAC) and the Multiband Imaging Photometer for *Spitzer* (MIPS). IRAC images were obtained on 2004 Dec 19, with MIPS imaging occurring on 2005 Apr 8. Results for N103B from this observing campaign were first published as part of an infrared SNR atlas of the LMC by Seok et al. (2013), who report a flux at

24 μm of 0.505 Jy. The remnant is small enough (30'' in diameter) to easily fit within the FOV of all of *Spitzer's* instruments. The spatial resolution of *Spitzer* is 1''–2'' for the IRAC arrays, $\sim 7''$ for the 24 μm camera, and 20'' at 70 μm . Our IRAC observations consisted of a dither pattern of five pointings with a frame time of 30 seconds for each frame. MIPS observations depended on the camera used. At 24 μm , we mapped the remnant with 44 overlapping pointings of 10 s each. At 70 μm , we mapped it with 94 pointings of 10 s each. The 160 μm map consisted of 252 pointings of 3 s. As the 160 μm images show only emission from the ISM with no discernable emission from the remnant, we do not discuss them further. Likewise, no obvious emission is seen at wavelengths at 100 μm or beyond in archival *Herschel* data. All *Spitzer* data have been processed with the *Spitzer* Post-Basic Calibrated Data pipeline, version 19.0.

We used the Image Co-addition with Optional Resolution Enhancement (ICORE) software to deconvolve the 24 μm image. ICORE is publicly available via the web¹¹, and is designed for infrared astronomy. We processed our 24 μm data with the software, which uses the known PSF of *Spitzer* and all the individual frames that go into making a mosaic to deconvolve the image. Because we had such good coverage of the remnant with our 44 overlapping frames, we were able to obtain a resolution of $\sim 2''$ (based on measuring the FWHM of several point sources in the field). This allows for a more detailed comparison with X-ray and optical images of the remnant.

Spectroscopic observations with the Infrared Spectrograph (IRS) were obtained on 2008 Apr 26 as part of Program ID 40604. We mapped the remnant using the long-wavelength (14–38 μm), low-resolution ($\delta\lambda/\lambda$ 64–128) (LL) spectrograph. We stepped across the remnant in eight LL slit pointings, stepping perpendicularly 5.1'' each time. This step size is half the slit width and is also the size of a pixel on the LL instrument. We then shifted the slit positions by 56'' in the parallel direction and repeated the map, ensuring sufficient redundancy for each spatial location. This process was repeated for each of the two orders of the spectrograph. For the shorter wavelength

¹¹<http://web.ipac.caltech.edu/staff/fmasci/home/icore.html>

order (14-21 μm), each pointing consisted of two cycles of 30 s integration time. The longer wavelength order (where the remnant is brighter) consisted of two cycles of 14 s integration times. We also obtained short-wavelength (5.2-14.5 μm), low-resolution (SL) spectroscopy of a few select locations in the remnant. The choice of these locations was guided by our imaging observations from 2005. We use the IRS contributed software *CUBISM*¹² (Smith et al. 2007) to extract 1-D spectra from both the source and the background. For the spectra shown here, we subtract off a global background obtained by extracting simultaneous off-source spectra from either side of the remnant and averaging them together.

Additionally, we used the IRS Peak-up array at 16 μm to obtain an image of the remnant at $\sim 4''$ resolution. The Peak-up mapping consisted of a dithered map of five pointings, where each pointing was made up of four 30 s integration images. Because we already had an image at 24 μm , we did not use the 22 μm Peak-up camera. All *Spitzer* MIPS and Peak-up images are shown in Figure 1.

2.1. Optical Observations

Optical observations of N103B were carried out from the 1.5 m telescope at CTIO in 1994. These included narrow-band images in $\text{H}\alpha$, $[\text{S II}]\lambda\lambda 6716,6731$, and $[\text{O III}]\lambda 5007$, plus red and green continuum filters for subtracting the stars, as detailed in Table 1. The images were processed, including bias subtraction, flat-fielding, combining, and re-projection onto a common world coordinate system using standard IRAF¹³ techniques. The continuum frames were then subtracted from the emission-line ones (green from $[\text{O III}]$, and red from $\text{H}\alpha$ and $[\text{S II}]$), and the subtracted images were flux-calibrated using standard stars from Hamuy et al. (1992). The seeing

¹²<http://irsa.ipac.caltech.edu/data/SPITZER/docs/dataanalysis/tools/cubism/>

for all the observations was about $1''.6$.

The continuum-subtracted image (in all three lines, displayed in colors indicated in the caption), is shown in Figure 2. The filament shown in red that wraps around the entire western portion of the shell is quite faint and appears only in $H\alpha$, the likely signature of a nonradiative shock, while the much brighter knots that appear yellow are almost equally strong in $[S\ II]$ and $H\alpha$, indicating that here the shocks have become radiative in much denser material. The very bright white knot (indicated in Figure 2) is strong in all three lines, as well as in the infrared.

3. Results and Analysis

In Figure 1, we show the results of our IR imaging observations. From a circular aperture $40''$ in diameter, we measure a $24\ \mu\text{m}$ flux of 0.48 Jy. By experimenting with several different background apertures, we can get a measure of the statistical error on the flux, which we find to be only 2%. The remnant is extremely bright at $24\ \mu\text{m}$, particularly compared to the surrounding ISM, which itself is quite uniform. The *MIPS Instrument Handbook* lists calibration uncertainties on fluxes of extended sources at 4%, so our overall uncertainty should be $\lesssim 0.03$ Jy. The $[O\ IV]/[Fe\ II]$ line complex at $26\ \mu\text{m}$ contributes a negligible flux when the spectrum is integrated over the wide MIPS $24\ \mu\text{m}$ bandpass; i.e., virtually all of the emission seen is from dust. Our flux measurement is within errors of that from Seok et al. (2013). We list all fluxes in Table 2.

At $16\ \mu\text{m}$, the remnant is still quite bright. We measure a flux of 0.19 Jy, with statistical uncertainties of 4%. The *IRS Data Handbook* reports systematic uncertainties of 6% on measured fluxes from the Peak-Up array, so combined in quadrature with our measurement uncertainties, we find an overall uncertainty in the $16\ \mu\text{m}$ flux of 0.014 Jy. For both the 24 and $16\ \mu\text{m}$ fluxes,

¹³IRAF is distributed by the National Optical Astronomy Observatories, which is operated by the AURA, Inc. under cooperative agreement with the National Science Foundation.

we have used the images from the *Wide-Field Infrared Survey Explorer* (WISE) archive as a cross-calibration. At 22 and 12 μm , we measure fluxes of 0.41 and 0.13 Jy, respectively.

At 70 μm , the situation becomes more complicated. The PSF of the telescope is less than the diameter of the remnant, but only barely. However, the background surrounding N103B emission is quite complex at 70 μm , as is shown in Figure 1. Throughout the MIPS 70 μm field of view, the surface brightness levels in the image vary from $\sim 30\text{--}130$ MJy/sr. At the location of the remnant, there is a peak in the emission, but other peaks of comparable brightness exist that are unrelated to the remnant, most notably to the E and SW. Using aperture photometry with varying background regions, we obtain fluxes ranging from 0.04 to 1.3 Jy. Given this extremely large spread, we conclude that while there likely is very faint emission from the remnant at this wavelength, the flux measurement itself is not reliable enough to be used as a constraint in modeling the dust in the remnant. We consider the highest value measured, 1.3 Jy, to be an upper limit to the flux at 70 μm .

In Figure 2, we show the results of our IRAC imaging. In the individual IRAC bands, there is no obvious emission from the remnant. However, a three-color image, with the 8.0 μm , 5.6 μm , and 4.5 μm images shown in red, green, and blue, respectively, does bring out emission that not only has slightly different colors than the ambient ISM, but also corresponds morphologically with the optical emission from the radiative shocks, as traced by [S II], also shown in Figure 2.

In Figure 3, we show the spatially integrated LL spectrum of N103B. The spectrum is clearly dominated by continuum emission from warm dust, and in many ways, looks similar to the spectra from two other young remnants of Type Ia SNe in the LMC: 0509-67.5 and 0519-69.0 (Williams et al. 2011). However, unlike these two remnants, N103B shows line emission from low ionization states of various elements. [Fe II] lines at 18.7 and 24.3 μm are identifiable, and it is likely that most of the line at 26 μm is due to [Fe II] as well (the 26 μm Fe line blends with an [O IV] line at 25.9 μm at this spectral resolution, and we do not have high-resolution IR spectra to separate them). Lines from [Ne III] at 15.5 μm and [Si II] at 34.8 μm are also easily identifiable

in the spectrum; the spike at $\sim 38 \mu\text{m}$ is an instrumental artifact. It is not surprising to see such lines in the spectrum of N103B (and not 0509-67.5 or 0519-69.0), because N103B is known to have some radiative shocks (see Figure 2), whereas the other two young remnants are still purely in a nonradiative phase (Tuohy et al. 1982; Smith et al. 1991). For comparison, we also show the spectrum from the NW region of Kepler’s SNR (Williams et al. 2012). The similarities between the two spectra are obvious. Both show emission from silicate dust, as evidenced by the broad feature at $18 \mu\text{m}$ which manifests itself as a “shoulder” in the spectrum.

3.1. Dust Modeling

In Williams et al. (2012), we showed that heating of dust grains in Kepler by photons from the radiative shocks is insufficient to heat grains to the emitting temperatures observed. Even with unphysical assumptions, such as 100% of the shock energy being converted into UV photons, heating by this mechanism can only heat grains to at most 50 K (dust temperatures in N103B, as in Kepler, are much higher than this at around $\sim 115 - 130$ K). Collisional heating is required for such hot dust. Collisional heating in the slow, radiative shocks is insufficient to heat grains to the high observed temperatures required to emit in the mid-IR, as shown in Dwek (1987). Only the plasma conditions of the nonradiative, X-ray emitting shocks, traced in the optical by $\text{H}\alpha$ emission, provide an environment for grains to be heated to such temperatures. This implies a morphological correlation between these different energy regimes. We do observe such a correlation; see Section 3.4 for more discussion on this.

To model the dust emission observed, we use the models described by Borkowski et al. (2006) and follow the procedures used by Williams et al. (2011) and Williams et al. (2012). Briefly, grains are heated via collisions with hot ions and electrons in the post-shock plasma (the same hot plasma that emits thermal X-rays), where the final grain temperatures are a function of both the plasma temperature and density (the stronger dependence). We include effects from the

gradual erosion of grains due to sputtering. The type of dust is a parameter as well, and due to the fact that we clearly see the 18 μm silicate dust emission feature, we have opted to use standard “astronomical silicates,” with optical constants taken from Draine & Lee (1984). As in Kepler, we see no evidence for crystalline silicate features, such as those seen in the spectra around cool, evolved O-rich stars (Morris et al. 2008; Henning et al. 2010).

The X-ray plasma parameters are taken from Lewis et al. (2003), who list average values of the electron temperature and ionization timescale of the plasma in N103B of 1 keV and $10^{11} \text{ cm}^{-3} \text{ s}$, respectively. Though we do not have a direct measure of the ion temperature, we use an approximate value of 5 keV. This is slightly lower than the temperature we used in Kepler (8.9 keV), but given that N103B is slightly more evolved than Kepler, it is reasonable to assume the ion temperature will be lower. We stress here that the plasma temperature is the least sensitive parameter in collisional heating; see Williams et al. (2013) for a fuller discussion of the weak dependence of the dust spectrum on both the ion and electron temperature. If we had used the same proton temperature as in Kepler (almost a factor of two higher), our derived density would be lower by only 20%.

We use a χ^2 minimization algorithm to fit the spectrum from 21 to 33 μm , which we have found to be the most reliable region of the spectrum to fit to obtain a gas density. We find a best-fit with a post-shock density of $n_H = 45 \text{ cm}^{-3}$. The reduced χ^2 value for this fit is close to 1 over the fitted region. We obtain a 90% confidence interval for our upper and lower limits (where $\Delta\chi^2 = 2.71$) of 40 and 49 cm^{-3} , respectively. We show the fit to the spectrum in Figure 4. This density is quite high, particularly compared to other Type Ia SNRs in the LMC (Borkowski et al. 2006) that are believed to be expanding into the ambient interstellar medium (ISM). We discuss possible explanations for this in Section 4. In this model, 51% of the dust is destroyed via sputtering, the process of gradually liberating material from the surface of the grain via collisions with energetic ions (Draine & Salpeter 1979). We require a current dust mass

of $1.5 \times 10^{-3} M_{\odot}$. Accounting for the amount lost due to grain destruction, the total swept up dust mass in the remnant is $3 \times 10^{-3} M_{\odot}$. For a standard LMC dust-to-gas ratio of 2.5×10^{-3} (Weingartner & Draine 2001), this leads to a swept-up gas mass of $1.2 M_{\odot}$. However, previous studies (Borkowski et al. 2006; Williams et al. 2006) have shown that the dust-to-gas ratio as determined from mid-IR observations of SNRs can be lower than the canonical value by a factor of a few, so the actual swept-up gas mass in N103B is likely a few solar masses.

3.2. 18 μm Silicate Feature

As in Kepler, our dust models have no trouble fitting the continuum beyond 20 μm , but between 15 and 20 μm , the model underpredicts the observed emission. This is the region of the spectrum where the “18 μm ” silicate feature is observed (Draine & Lee 1984). Despite the fact that our silicate grain model does include this feature, it still fails to reproduce the observed spectrum in this region because the “18 μm ” feature is not, in fact, at 18 μm . Again, as is the case with Kepler, the silicate feature is located at approximately 17.3 μm . We find this by following the technique of Guha Niyogi et al. (2011) of fitting a blackbody model to the underlying continuum and dividing this out of the spectrum. What remains is the absorption efficiency of the silicate dust grains as a function of wavelength, which we show in Figure 5.

There is no dust temperature at which the optical constants of Draine & Lee (1984) can account for the observed features. There are examples in the literature of variation in the location of the silicate feature. Ossenkopf et al. (1992) note that there are differences between silicates in the CSM and ISM, since circumstellar dust is modified by processing within the ISM. This suggests the possibility that the dust we are seeing would be newly-formed dust from the outflow from the progenitor that has not yet been reprocessed within the ambient ISM. Henning et al. (2010) report variations in silicate features seen from the spectra of AGB stellar outflows. Additionally, Smith et al. (2010) find that the “18 μm ” feature in the nucleus of M81 is actually at

17.2 μm , similar to our observed location.

3.3. X-ray Modeling

The presence of O lines in the *XMM-Newton* RGS grating spectrum is reported by Van der Heyden et al. (2002). These authors inferred from this that the progenitor must have been a core-collapse SN from a massive star. They report a value of $0.27 M_{\odot}$ of O assuming a density that is a few times higher than that which we report here. With the density in the post-shock environment now determined from our IR observations reported, we can easily reconcile the presence of O lines with the fact that N103B is now known to be a SN Ia. The higher densities we find lower the mass of O implied by the fits of Van der Heyden et al. (2002). It is beyond the scope of this paper to do our own detailed spectral fitting to the X-ray data, but we note that it is also possible that some of the O lines come from the ejecta; e.g., the canonical “W7” model of Nomoto et al. (1984) produces $0.14 M_{\odot}$ of O. However, Lewis et al. (2003) use the high-resolution *Chandra* data to conclude that it is unlikely that the O component of the spectrum originates within the ejecta. The bulk of the O emission seen likely comes from the interaction of the forward shock with the dense circumstellar material. X-ray O emission arises quite easily in shocked gas, and even the remnant of SN 1006 (widely known to be the remnant of a Type Ia SN) shows substantial O lines in its X-ray spectrum (Winkler et al. 2014), which may arise from ejecta or shocked ISM.

Detailed X-ray spectral modeling is beyond the scope of this paper, but we have fit models to the integrated RGS X-ray spectrum to determine the shocked gas mass in the remnant. We fit both a plane-shock model and a Sedov model. For an assumed absorption column of $2.5 \times 10^{21} \text{ cm}^{-2}$, we derive emission measures of 1.3 and $1.5 \times 10^{59} \text{ cm}^{-3}$ for the plane-shock and Sedov models, respectively. With our measured post-shock density of 45 cm^{-3} , we derive a total swept-up mass of $2.7\text{-}3.3 M_{\odot}$. While only a rough estimate, this number agrees relatively well with our inferred

gas mass from the assumed dust-to-gas mass ratio.

3.4. Multi-Wavelength Comparison

In Figure 2, we show a three-color optical image of N103B at $\sim 1.8''$ resolution. Only the western hemisphere of the remnant is visible, with the entire forward shock emitting in $H\alpha$. As we mentioned in Section 2.1, this is strongly suggestive that the Balmer emission observed in N103B arises from nonradiative shocks over a significant portion of the remnant.

A few arcseconds interior to the forward shock are several knots that also emit in [S II] and [O III], tracers of regions where the shocked material has cooled significantly and the shocks have become radiative. The brightest knot in the remnant at all three optical wavelengths (approximately halfway in between the north and south boundaries), which appears unresolved in the image, is also seen in the IRAC data, also shown in Figure 2. The source of this emission is not clear, but is likely due to radiative cooling lines in the near-IR. We show, in Figure 6, the short-low spectrum from this knot, which reveals an Ar II line at $7 \mu\text{m}$. The IRS cuts off at $\sim 5.5 \mu\text{m}$, so the source of the emission at IRAC channels 2 and 3 (4.5 and $5.6 \mu\text{m}$) cannot be identified from the spectra available.

In Figure 7, we show an optical image in [S II] and [O III], highlighting only the portions of the remnant where the shocks have become radiative. Contours of the $24 \mu\text{m}$ emission overlaid on top of these shocks shows only a weak correlation between the emission from warm dust and the cooler, radiative shocks. We also show in that Figure an $H\alpha$ image highlighting the Balmer-dominated portions of the shock. The correlation with the MIPS $24 \mu\text{m}$ emission is much stronger, consistent with what has been seen in other remnants resulting from both types of SNe, both young, like Kepler (Blair et al. 2007), and old, like the Cygnus Loop (Sankrit et al. 2010). This correlation confirms the presence of nonradiative, Balmer-dominated shocks in N103B.

While slow radiative shocks into dense clumps can heat dust, the much better morphological correlation with the $H\alpha$ emission means that the nonradiative shocks are the dominant heating source in this remnant.

Chandra X-ray images of N103B were first shown by Lewis et al. (2003). The ejecta of SNe Ia are rich in Fe, Si, and S, while not containing much O. In Figure 8, we show narrowband *Chandra* images centered on three different line emission bands: O, Fe, and Si+S, along with contours from the MIPS warm dust emission. Aside from the emission at all energies being brighter on the western side of the remnant, where the dust emission is also strongest, no obvious morphological comparison stands out between the dust emission and the Fe and Si + S bands. Since no dust has ever been observed in the ejecta of a Type Ia SN, this is not surprising. The best correlation with the $24\ \mu\text{m}$ dust comes from the 0.5-0.75 keV X-rays, containing significant O emission. Most of this emission arises from the interaction of the forward shock with the CSM.

Interestingly, the brightest X-ray knots of O emission correspond nearly perfectly to the bright optical [O III] knots, as we show in Figure 9. The optically-emitting knots arise from the densest regions of the CSM, and are where the shocks have become radiative. The correlation implies that there are multiple shocks present in these dense clumps; some dense and cool enough to provide significant optical emission, and some fast and hot enough for X-ray emission.

3.5. Asymmetry

Perhaps the most obvious feature of the remnant at all wavelengths is the asymmetry between the E and W halves. Stellar winds, by themselves, cannot easily reproduce such an asymmetry. While winds can be anisotropic, they should still be symmetric in either the polar or equatorial direction. Here, again, we are reminded of Kepler, which is a factor of several brighter in the N hemisphere than the S (Blair et al. 2007). Kepler, located well out of the Galactic plane where

densities are $\sim 10^{-2.5} - 10^{-3} \text{ cm}^{-3}$ (McKee & Ostriker 1977), has a high systemic velocity of $\sim 300 \text{ km s}^{-1}$. In the model of Bandiera (1987), the asymmetry of Kepler is reproduced with a “comet” model, in which the mass losing star moving at relatively high velocity creates a bow shock from its interaction with the ISM.

N103B may not have the high spatial velocity of Kepler relative to the local ISM, but this is not necessary for a bow shock to form. As a rough calculation, the ram pressure (which scales as nv^2 , where n is the ISM density and v the velocity of the system) from the ISM resulting from a 300 km s^{-1} star moving through an ISM with $n = 1 \times 10^{-3} \text{ cm}^{-3}$ (appropriate for Kepler) is equivalent to the pressure exerted by an ISM with $n = 1 \text{ cm}^{-3}$ on a system moving at 10 km s^{-1} . Hydrodynamic simulations of Villaver et al. (2012) show that bow shocks with significant density differences between the direction of motion and the trailing direction can form in the winds of AGB stars with velocities as low as 10 km s^{-1} in densities as low as 0.1 cm^{-3} . Many such systems have been observed with *Herschel*; see Jorissen et al. (2011) for examples.

4. Discussion

The density we derive is very close to what was found for Kepler’s SNR (Williams et al. 2012), unsurprising given the similarities between the two spectra. As we show in Table 3, this density is an order of magnitude or more higher than any other Type Ia remnants. What could account for such a high density? One possibility is a coincidental encounter of the shock in the W hemisphere with a dense interstellar cloud. However, this explanation would not explain the shape of the remnant as being round and reminiscent of a bow shock nebula. Additionally, the $18 \mu\text{m}$ feature of silicate dust in dense interstellar clouds is actually at $18 \mu\text{m}$ (in fact, the optical properties of silicate grains which place the location of the feature at $18 \mu\text{m}$ are usually determined from observations of such clouds).

A more straightforward explanation is the same one invoked for Kepler: N103B is expanding into a dense CSM ejected from the progenitor system prior to explosion. This would explain the high densities and the formation of a bow shock nebula. An obvious question that arises from this is what the progenitor was. In Kepler, an AGB star has been favored by several authors, but there is an issue with an AGB interpretation for N103B. The atmospheres of massive AGB stars should be overabundant in N (Marigo et al. 2011), particularly at LMC metallicities (Karakas 2003), but the optical spectra of N103B do not show such an N enhancement (Russell & Dopita 1990). This can be taken as evidence that the WD companion had not undergone the first dredge-up prior to the pre-SN mass loss. Explanations other than the symbiotic AGB progenitors have been invoked to account for objects such as SN 2002ic, a Type Ia with the dense CSM. In the models of Han & Podsiadlowski (2006) (see also similar models in Meng & Yang (2010)), material from a companion star is lost prior to the first dredge-up and the RGB and AGB phases of the stellar evolution.

Whatever the interpretation of the dense material in N103B, an additional issue is that with an ionization timescale from a plane-shock model for the X-ray emitting gas of $10^{11} \text{ cm}^{-3} \text{ s}$ (Lewis et al. 2003), our fitted post-shock density leads to a shock age of $\sim 60 \text{ yr}$. We expect a shock age of $\sim 300 \text{ yr}$, since the “effective” age in Sedov dynamics for a plane-shock model is about 1/3 the true age of the remnant (Borkowski et al. 2001). One possibility is that this ionization timescale is too short; Van der Heyden et al. (2002) give a value of $2.3 \times 10^{11} \text{ cm}^{-3} \text{ s}$. Using this, our shock age would be 140 yr. Another possibility is that the remnant is younger than the best-fit age of 870 yr reported in Rest et al. (2005). The authors there give a lower limit of 380 yr, a value that would further reduce the discrepancy by a factor of two. While this SN would have been easily visible from Earth with the naked eye, there is no documented historical record. However, this is not necessarily a problem, as another SN Ia in the LMC with an age determined from light echoes, SNR 0509-67.5 (an age of $\sim 400 \text{ yr}$), also has no documentation of its SN event. Badenes et al. (2008) present an interesting discussion of the lack of a historical record for

0509-67.5 in the context of exploration and colonization of the southern hemisphere.

Since the remnant is basically unresolved in the spectroscopic observations, where our 3-D spatial-spectral cube has a spatial resolution of $> 10''$ beyond $30 \mu\text{m}$, another possible resolution to this is that we are seeing a superposition of various physically distinct emitting regions. This is the case in Kepler, where the density varies significantly throughout the remnant (Williams et al. 2012). As we showed for Kepler, dust emission at short wavelengths is dominated by nonradiative shocks driven into denser than average material, while at longer wavelengths, faster shocks into less dense material will dominate. Unfortunately, this hypothesis is not testable for N103B with current data. As we stated in Section 2, flux measurements at $70 \mu\text{m}$ are unreliable, and no emission at longer wavelengths is seen from *Herschel*. In the near future, the only reasonable observational test of this in the IR would be much higher spatial-resolution IR spectra. This will be possible with the *James Webb Space Telescope (JWST)*. Even though JWST will only go out to $\sim 25 \mu\text{m}$, one could still search on arcsecond scales for variations in the shape of the continuum emission, a clear indication of varying dust temperatures, and thus, varying densities.

5. Conclusions

The LMC remnant N103B shows strong emission in the mid-IR from warm dust grains in the post-shock environment. Its luminosity at $24 \mu\text{m}$ is nearly an order of magnitude higher than any other known Type Ia SNR. The spectrum is virtually identical to that seen from Kepler’s SNR, which is known to be interacting with a dense CSM. We propose that N103B is a more evolved version, i.e., an “older cousin,” of Kepler. We have several lines of circumstantial evidence for a circumstellar medium. The densities observed are substantially higher than any other Type Ia remnant known (with the exception of Kepler), either in the Galaxy or the LMC. The “ $18 \mu\text{m}$ ” feature of silicate dust is clearly different from other silicate dust observed in the ISM, possibly indicating that it has not yet been processed by the ISM. The shape of the remnant, strongly

indicative of a bow-shock formation in the W, requires an outflow from the progenitor system.

This interpretation is not without issues. The densities observed imply a very young shock (or a very recent shock interaction), lower by a factor of several from what is expected. A younger age and/or lower densities in the nonradiative shocks would alleviate this. Whereas Kepler has been interpreted as having an AGB star in the progenitor system, the overabundance of N in the optical spectrum predicted for massive AGB stars is not observed in N103B. However, the detailed relationship between the time evolution of N production in the progenitor system and the time of the SN explosion is poorly understood. One solution to this is that it may not have been an AGB star in the progenitor system, but rather a star that experienced significant mass prior to the first dredge-up of material. Such an explanation has been invoked to explain the Type Ia SN 2002ic. Finally, it is entirely possible that we are seeing an unresolved mix of ISM and CSM gas, which would suppress any N enhancement in the optical spectra.

Alternative scenarios to the CSM interpretation are less appealing. One possibility to explain the high density observed would be a coincidental encounter of the shock in the W hemisphere with a dense interstellar cloud, but such a chance encounter would not necessarily solve the issues listed above. While this could explain the lack of N overabundance (since the dense gas would be of ISM origin, and not CSM), it would not explain the shape of the remnant as being round and reminiscent of a bow shock nebula. Additionally, the $18\ \mu\text{m}$ feature of silicate dust in dense interstellar clouds is actually at $18\ \mu\text{m}$ (in fact, the optical properties of silicate grains which place the location of the feature at $18\ \mu\text{m}$ are usually determined from observations of such clouds).

If the CSM interpretation is correct, N103B would become only the second known example of a Type Ia SN to be interacting with such a medium during the remnant phase. Such dense surroundings for the forward shock account for the strong O emission seen in the X-ray spectra. The strong E-W asymmetry is very similar to Kepler (where the asymmetry is N-S). A slowly moving progenitor system blowing a slow wind can give rise to such a geometry. Such winds

are most easily produced in a single-degenerate scenario. It is possible, though far from certain, that a companion star may still exist in the vicinity of N103B. However, because the lack of N abundance in the spectra disfavors an AGB or RGB star (both of which are quite bright), detecting such a companion star at 50 kpc may not be an easy task.

A dense CSM suggests that the SN that created N103B arose from a binary system containing a relatively young, massive progenitor. In an extragalactic population study, Aubourg et al. (2008) report significant evidence for a small population of short-lived SNe Ia progenitors with lifetimes less than 180 Myr and main-sequence masses in the range of $\sim 3.5 - 8 M_{\odot}$. Mannucci et al. (2006) also concluded that a population of “prompt” SNe Ia must exist (characterized by delay times from stellar birth to SNe of ~ 100 Myr). Badenes et al. (2009) note that the local environs of N103B are associated with a burst of star-forming activity, with a prominent extended peak between 100 and 50 Myr in the past. Their statistical analysis gives a 73% chance that a Type Ia SN in such a region would be a prompt Ia, and they note that a metal-rich progenitor is likely. *Spitzer’s* limited resolution does not allow for spatially-resolved spectroscopy, so the potential for future study in the mid-IR with the *James Webb Space Telescope* is clear. Better characterization of the X-ray emission, such as spectrally decomposing regions dominated by the forward-shocked CSM and the reverse-shocked ejecta on small spatial scales would be useful. A deep *Chandra* observation could accomplish this on scales similar to what will be observable with *JWST*.

Table 1. Imaging Observations of N103B from CTIO 1.5 m Telescope

Date	Filter			Exposure (s)	Observer
	Designation	λ_0 (Å)	$\Delta\lambda^a$ (Å)		
1994 Dec 7	[O III] λ 5007	5008	58	2×750	C. Smith
1994 Dec 7	Green Continuum	5133	100	2×500	C. Smith
1994 Jan 8	H α	6565	24	2×600	Winkler
1994 Dec 7	[S II] $\lambda\lambda$ 6716, 6731	6728	48	2×900	C. Smith
1994 Jan 8	Red Continuum	6848	94	2×400	Winkler

^aFWHM

Table 2. *Spitzer* IR Flux Measurements of N103B

Wavelength (μm)	Flux (Jy)
16	0.19 ± 0.014
24	0.48 ± 0.03
70	< 1.3

Note. — Background-subtracted fluxes measured from a circular aperture centered on the remnant, $40''$ in diameter. Uncertainties are combined statistical and systematic uncertainties; see text for details.

Table 3. Comparison of IR Emission from Type Ia SNRs

Object	n_H (cm ⁻³)	L_{IR}	$L_{24,50kpc}$
0548-70.4	1.7	2.1×10^{36}	2.63
0509-67.5	0.59	1.5×10^{36}	16.7
Tycho's SNR	0.4	5.4×10^{36}	73
DEM L71	2.3	1.2×10^{37}	88
0519-69.0	6.2	4.3×10^{36}	92
Kepler's SNR	42	2.8×10^{36}	95
N103B	45	8.4×10^{36}	480

Note. — n_H is post-shock density. L_{IR} is the luminosity, in units of ergs s⁻¹. $L_{24,50kpc}$ is the flux at 24 μ m, normlized to the LMC distance for Kepler and Tycho (assuming 5 kpc distance for Kepler and 3 kpc for Tycho.)

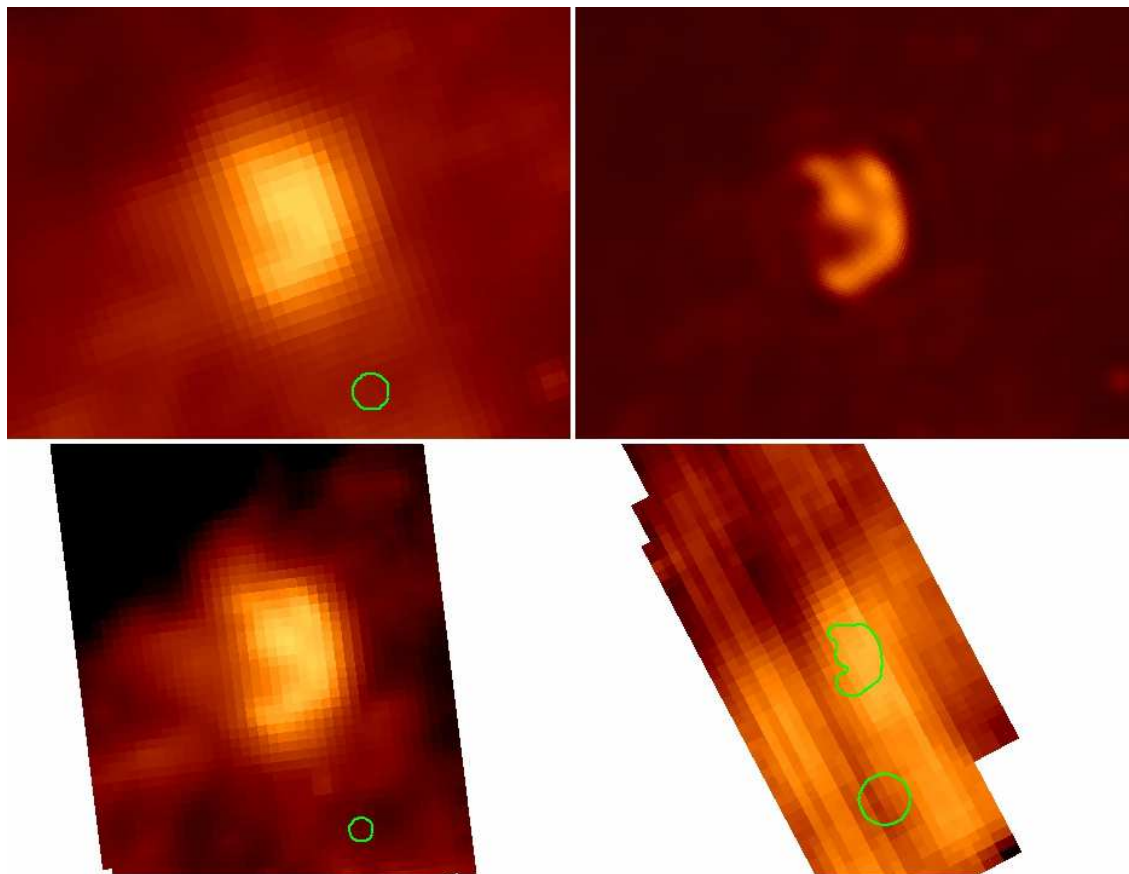


Fig. 1.— *Spitzer* images of N103B. *Top Left*: 24 μm image; *Top Right*: 24 μm image, deconvolved (see text for details); *Bottom Left*: 16 μm “Peakup” array image; *Bottom Right*: 70 μm image, zoomed out by a factor of two to show the surroundings of the remnant. A single 24 μm contour is overlaid. The native resolutions of all three instruments are shown as circles on their respective images. For all images here and in subsequent figures, north is up and east is to the left.

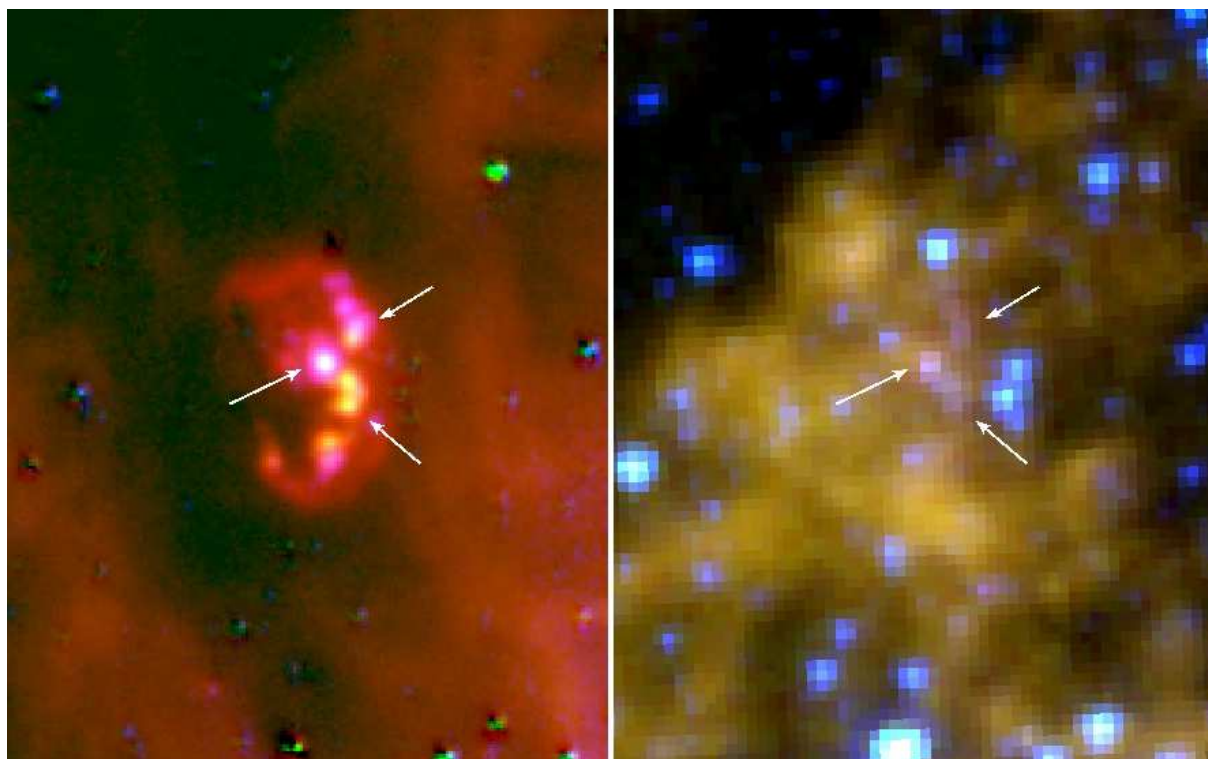


Fig. 2.— *Left*: Optical emission-line image of N103B, where red = $H\alpha$, green = [S II], and blue = [O III], in a display scaled as the square root of the intensity. The stars have been largely removed by subtracting scaled continuum images. *Right*: Three-color IRAC image, with 8.0 μm emission in red, 5.6 μm in green, and 4.5 μm in blue. The colors allow a distinction between emission (indicated with arrows) that is likely from the remnant and that of the general diffuse ISM. Both panels are on the same scale.

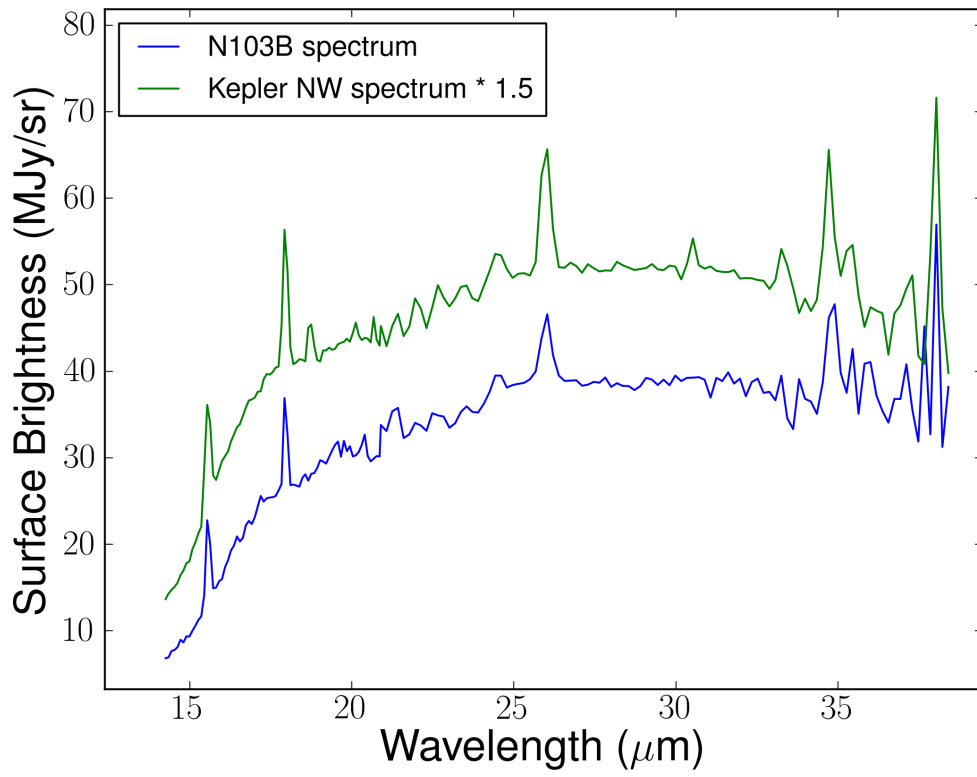


Fig. 3.— IRS LL spectra from N103B and the NW region of Kepler’s SNR. For display purposes, the spectrum from Kepler has been multiplied by a factor of 1.5.

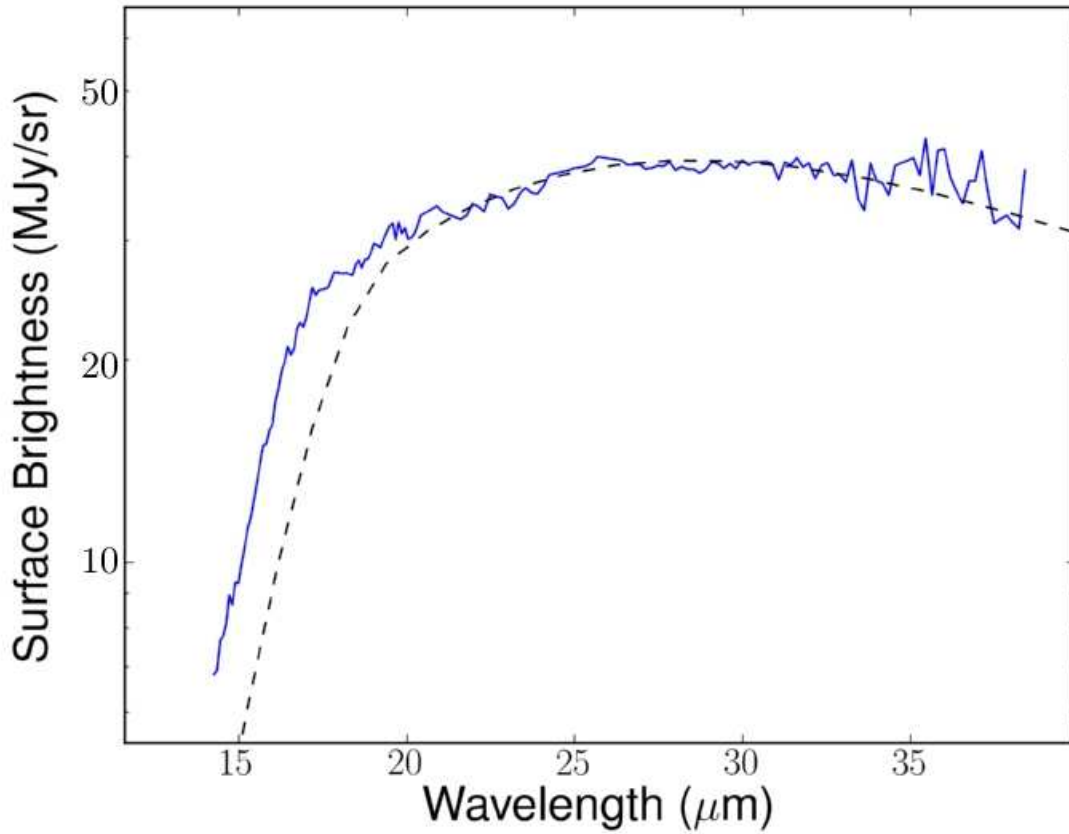


Fig. 4.— LL spectrum of N103B, overlaid with model fit with post-shock density, $n_H = 45 \text{ cm}^{-3}$. The spectrum is the same as that shown in Figure 3, except that the lines and bad pixels have been removed (to highlight the shape of the continuum) and the vertical axis is logarithmic. The model, which includes the $18 \mu\text{m}$ silicate feature, fails to reproduce the observed spectrum because the feature in N103B is not located at $18 \mu\text{m}$.

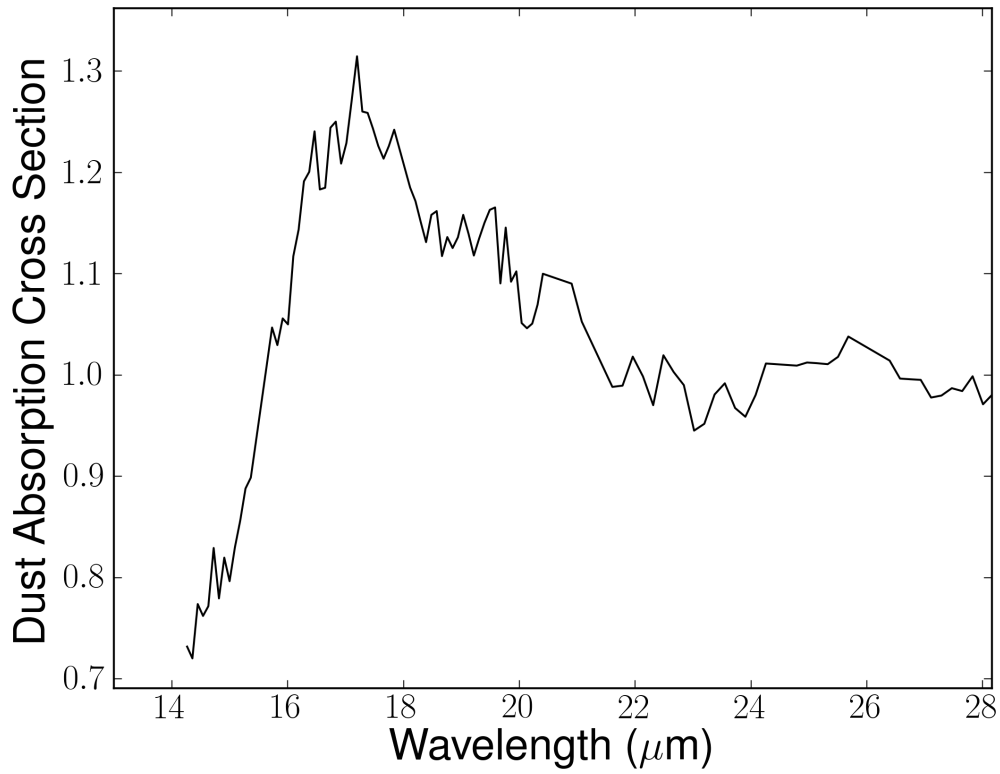


Fig. 5.— Absorption cross section of the dust in N103B obtained by dividing spectrum by black-body fit, as described in the text. The broad feature peaks at $17.3 \mu\text{m}$, rather than $18 \mu\text{m}$ like most interstellar silicate dust.

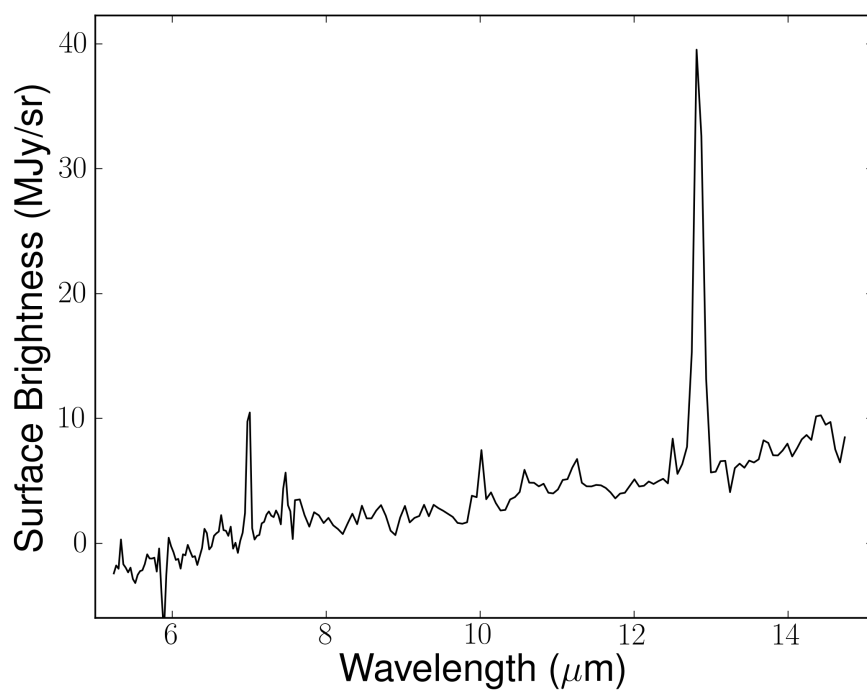


Fig. 6.— Background-subtracted short-low spectrum of the brightest emitting radiative knot in N103B. Lines of Ar ($7.0 \mu\text{m}$) and Ne ($12.8 \mu\text{m}$) are present.

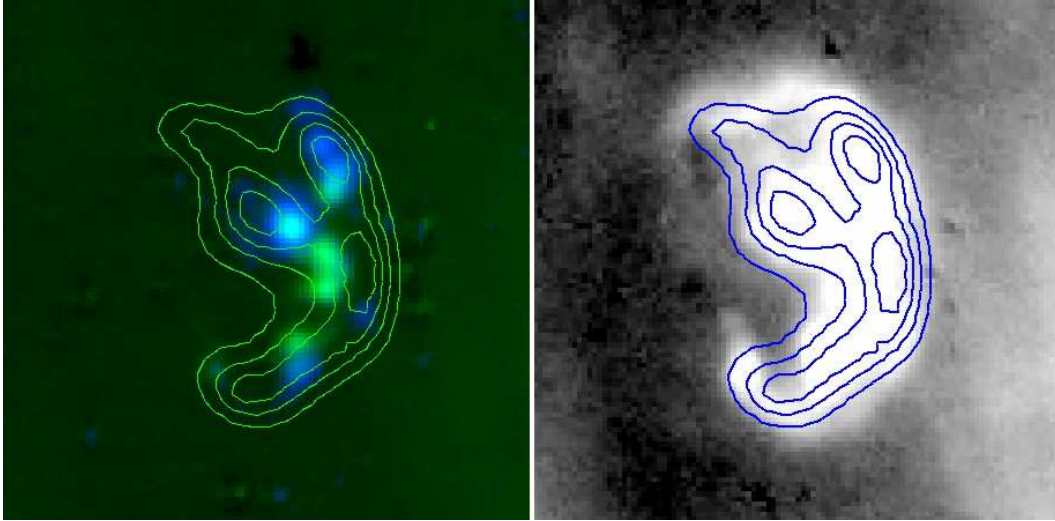


Fig. 7.— *Left*: Optical image with [S II] in green and [O III] in blue, with contours overlaid from deconvolved MIPS 24 μm image. There is little correlation between dust emission and radiative shock emission. *Right*: $\text{H}\alpha$ emission, stretched to show faintest nonradiative emission at forward shock, with the same MIPS contours overlaid.

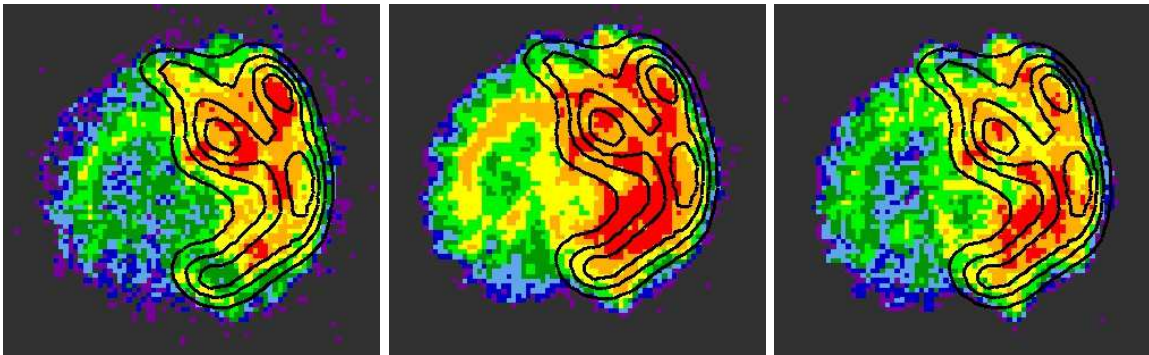


Fig. 8.— *Left*: 0.5-0.75 keV X-rays, containing O emission; *Center*: 0.75-1.2 keV X-rays, containing Fe emission; *Right*: 1.2-6 keV X-rays, containing Si and S emission. Contours from the MIPS 24 μm image are overlaid on each. All images have been slightly smoothed with a 1-pixel gaussian.

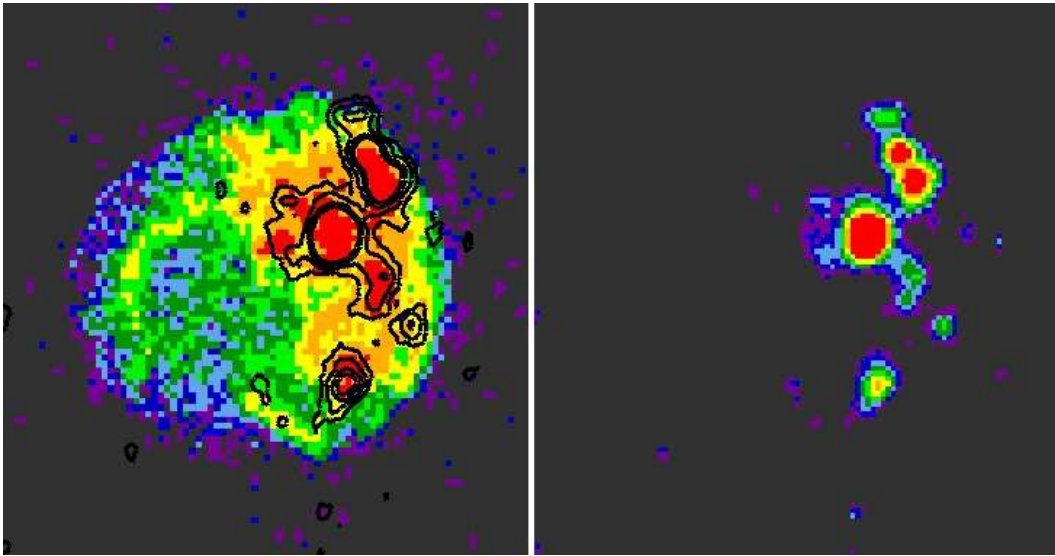


Fig. 9.— *Left*: 0.5-0.75 keV X-rays, containing O emission. *Right*: Optical [O III] image. Contours of [O III] emission are overlaid on the X-ray image, highlighting near perfect correlation of bright knots in both energy regimes.

REFERENCES

- Aubourg, E., Tojeiro, R., Jiminez, R., Heavens, A., Strauss, M.A., & Spergel, D.N. 2008, *A&A*, 492, 631
- Badenes, C., Hughes, J.P., Bravo, E., & Langer, N. 2007, *ApJ*, 662, 472
- Badenes, C., Hughes, J.P., Cassam-Chenai, G., Bravo, E. 2008, *ApJ*, 680, 1149
- Badenes, C., Harris, J., Zaritsky, D., Prieto, J.L. 2009, *ApJ*, 700, 727
- Blair, W.P., Ghavamian, P., Long, K.S., Williams, B.J., Borkowski, K.J., Reynolds, S.P., & Sankrit, R. 2007, *ApJ*, 662, 998
- Bandiera, R. 1987, *ApJ*, 319, 885
- Borkowski, K.J., Lyerly, W.J., & Reynolds, S.P. 2001, *ApJ*, 548, 820
- Borkowski, K.J., et al. 2006, *ApJ*, 642, 141
- Burkey, M.T., Reynolds, S.P., Borkowski, K.J., & Blondin, J.M. 2013, *ApJ*, 764, 63
- Draine, B.T. & Salpeter, E.E. 1979, *ApJ*, 231, 77
- Draine, B.T. & Lee, H.M. 1984, *ApJ*, 285, 89
- Dwek, E. 1987, *ApJ*, 322, 812
- Gilfanov, M. & Bogdan, A. 2010, *Nature*, 463, 924
- Guha Niyogi, S., Speck, A.K., & Onaka, T. 2011, *ApJ*, 733, 93
- Hamuy, M., Walker, A.R., Suntzeff, N.B., Gigoux, P., Heathcote, S.R., & Phillips, M.M. 1992, *PASP*, 104, 533
- Han, Z. & Podsiadlowski, Ph. 2006, *MNRAS*, 368, 1095

Henning, T. 2010, *ARA&A*, 48, 21

Hughes, J.P., et al. 1995, *ApJ*, 444, 81

Jorissen, A., et al. 2011, *A&A*, 532, 135

Karakas, A. 2003, PhD Thesis, Monash University

Katsuda, S., Long, K.S., Petre, R., Reynolds, S.P., Williams, B.J., & Winkler, P.F. 2013, *ApJ*, 763, 85

Kerzendorf, W.E., Childress, M., Scharwachter, J., Do, T., Schmidt, B.P. 2014, *ApJ*, 782, 27

Lewis, K.T., Burrows, D.N., Hughes, J.P., Slane, P.O., Garmire, G.P., & Nousek, J.A. 2003, *ApJ*, 582, 770

Lopez, L.A., Ramirez-Ruiz, E., Huppenkothen, D., Badenes, C., & Pooley, D.A. 2011, *ApJ*, 732, 114

Mannucci, F., Della Valle, M., & Panagia, N. 2006, *A&A*, 370, 773

Marigo, P., Bressan, A., Girardi, L., Aringer, B., Gullieuszik, M., & Groenewegen, M.A.T. 2011, in *Why Galaxies Care about AGB Stars II: Shining Examples and Common Inhabitants*, Eds. F. Kerschbaum, T. Lebzelter, and R.F. Wing. San Francisco: Astronomical Society of the Pacific, p. 431.

McKee, C.F. & Ostriker, J.P. 1977, *ApJ*, 218, 148

Meng, X. & Yang, W. 2010, *ApJ*, 710, 1310

Morris, P.W. 2008, in *IAU Symp. 250, Massive Stars as Cosmic Engines*, ed. F. Bresolin, P.A. Crowther, & J. Puis (Cambridge: Cambridge Univ. Press), 361

Nomoto, K., Thielemann, F.-K., & Yokoi, K. 1984, *ApJ*, 286, 644

Ossenkopf, V., Henning, Th., & Mathis, J.S. 1992, *A&A*, 261, 567

Rest, A., et al. 2005, *Nature*, 438, 1132

Rest, A., et al., in preparation

Reynolds, S.P., Borkowski, K.J., Hwang, U., Hughes, J.P., Badenes, C., Laming, J.M., & Blondin, J.M. 2007, *ApJ*, 668, 135

Russell, S.C. & Dopita, M.A. 1990, *ApJS*, 74, 93

Sankrit, R., et al. 2010, *ApJ*, 712, 1092

Schaefer, B.E. & Pagnotta, A. 2012, *Nature*, 481, 164

Seok, J.-Y., Koo, B.-C., & Onake, T. 2013, *ApJ*, 779, 134

Silverman, J.M., et al. 2013, *ApJS*, 207, 3

Smith, R.C., Kirshner, R.P., Blair, W.P., & Winkler, P.F. 1991, *ApJ*, 375, 652

Smith, J.D.T., et al. 2007, *PASP*, 119, 1133

Smith, H.A., et al. 2010, *ApJ*, 716, 490

Someya, K., Bamba, A., & Ishida, M. 2013, arXiv:1310.4244

Tuohy, I.R., Dopita, M.A., Mathewson, D.S., Long, K.S., & Helfand, D.J. 1982, *ApJ*, 261, 473

Van der Heyden, K.J., Behar, E., Vink, J., Rasmussen, A.P., Kaastra, J.S., Bleeker, J.A.M, Kahn, S.M., & Mewe, R. 2002, *A&A*, 392, 955

Villaver, E., Manchado, A., & Garcia-Segura, G. 2012, *ApJ*, 748, 94

Wang, B. & Han, Z. 2012, *New Astron. Rev.*, 56, 122

Waters, L.B.F.M. 2011, in ASP Conf. Ser. 445, Why Galaxies Care About AGB Stars II: Shining Examples and Common Inhabitants, ed. F. Kerschbaum, T. Lebzelter, & R.F. Wing (San Francisco, CA: ASP), 227

Weingartner, J.C., & Draine, B.T. 2001, ApJ, 548, 296

Williams, B.J., et al. 2006, ApJ, 652, 33

Williams, B.J., et al. 2011, ApJ, 729, 65

Williams, B.J., et al. 2011, ApJ, 741, 96

Williams, B.J., Borkowski, K.J., Reynolds, S.P., Ghavamian, P., Blair, W.P., Long, K.S., & Sankrit, R. 2012, ApJ, 755, 3

Williams, B.J., et al. 2013, ApJ, 770, 129

Winkler, P.F., Williams, B.J., Blair, W.P., Borkowski, K.J., Ghavamian, P., Long, K.S., Raymond, J.C., & Reynolds, S.P. 2013, ApJ, 764, 156

Winkler, P.F., et al. 2014, ApJ, 781, 65

Yang, X.J., Tsunemi, H., Lu, F.J., Li, A., Xiang, F.Y., Xiao, H.P., & Zhong, J.X. 2013, ApJ, 766, 44